Received: 18 August 2022 | Accepted: 3 February 2023

DOI: 10.1111/jvim.16654

STANDARD ARTICLE

Journal of Veterinary Internal Medicine Open Access

ACVIM American College of Veterinary Internal Medicine

Quantitative analysis of magnetic resonance images for characterization of blood-brain barrier dysfunction in dogs with brain tumors

Erez Hanael[1] | Shelly Baruch[1] | Orit Chai[1] | Liron Lishitsky[1] | Tal Blum[1] | Kira Rapoport[1] | Marco Ruggeri[1] | Zahi Aizenberg[1] | Dana Peery[1] | Nina Meyerhoff[2] | Holger Andreas Volk[2] | Steven De Decker[3] | Andrea Tipold[2] | Wolfgang Baumgaertner[2] | Alon Friedman[4,5] | Merav Shamir[1]

[1]The Koret School of Veterinary Medicine, Neurology and Neurosurgery, Hebrew University of Jerusalem, Reehovot, Israel

[2]School of Veterinary Medicine Hannover, Small Animal Medicine and Surgery, Hannover, Germany

[3]Department of Clinical Sciences, Royal Veterinary College, University of London, Hertfordshire, UK

[4]Faculty of Medicine, Department of Medical Neuroscience Halifax, Dalhousie University, Nova Scotia, Canada

[5]Departments of Physiology and Cell Biology, Brain, and Cognitive Sciences, Zlotowski Center for Neuroscience, Ben-Gurion University of the Negev, Beer-Sheva, Israel

Correspondence
Merav Shamir, The Koret School of Veterinary Medicine, Neurology and Neurosurgery, Hebrew University of Jerusalem, Reehovot, Israel.
Email: merav.shamir@mail.huji.ac.il

Funding information
ISF- Israel Science Foundation, Grant/Award Number: 717/15

Abstract

Background: Blood-brain barrier (BBB) permeability can be assessed quantitatively using advanced imaging analysis.

Hypothesis/Objectives: Quantification and characterization of blood-brain barrier dysfunction (BBBD) patterns in dogs with brain tumors can provide useful information about tumor biology and assist in distinguishing between gliomas and meningiomas.

Animals: Seventy-eight hospitalized dogs with brain tumors and 12 control dogs without brain tumors.

Methods: In a 2-arm study, images from a prospective dynamic contrast-enhanced (DCE; n = 15) and a retrospective archived magnetic resonance imaging study (n = 63) were analyzed by DCE and subtraction enhancement analysis (SEA) to quantify BBB permeability in affected dogs relative to control dogs (n = 6 in each arm). For the SEA method, 2 ranges of postcontrast intensity differences, that is, high (HR) and low (LR), were evaluated as possible representations of 2 classes of BBB leakage. BBB score was calculated for each dog and was associated with clinical characteristics and tumor location and class. Permeability maps were generated, using the slope values (DCE) or intensity difference (SEA) of each voxel, and analyzed.

Results: Distinctive patterns and distributions of BBBD were identified for intra- and extra-axial tumors. At a cutoff of 0.1, LR/HR BBB score ratio yielded a sensitivity of 80% and specificity of 100% in differentiating gliomas from meningiomas.

Conclusions and Clinical Importance: Blood-brain barrier dysfunction quantification using advanced imaging analyses has the potential to be used for assessment of brain tumor characteristics and behavior and, particularly, to help differentiating gliomas from meningiomas.

Abbreviations: BBB, blood-brain barrier; BBBD, blood-brain barrier dysfunction; CNS, central nervous system; CSF, cerebrospinal fluid; DCE-MRI, dynamic contrast-enhanced MRI; IAUGC, initial area under the gadolinium curve; SEA, subtraction enhancement analysis.

KEYWORDS
blood-brain barrier, CNS disorders, epilepsy, glioma, meningioma, neurology, structural epilepsy

1 | INTRODUCTION

Intracranial neoplasia is common in dogs, with older age and body weight of above 15 kg being risk factors for the occurrence of meningiomas and a prevalence of 4.5% in dogs undergoing postmortem examination.[1] The most common primary brain tumor in dogs is meningioma, which represents 50% of all diagnosed tumors, followed by gliomas, representing 30% to 40%.[1-3] Each of these tumor classes has unique biological characteristics and behavior, which influence prognosis and treatment options.[4,5] Thus, identifying tumor class is essential for appropriate treatment planning and management. However, identification is not always possible, even when high-field magnetic resonance imaging (MRI) is available.[6]

Magnetic resonance imaging features associated with meningiomas include broad-based attachment to the meninges, meningeal tail, distinct tumor margins, and uniform contrast enhancement in T1-weighted sequences. In addition, peritumoral edema is present in >90% of the cases.[6,7] A study of 40 dogs reported 85% accuracy of correctly identified meningiomas by MRI.[6] Gliomas originate within the brain parenchyma and are the most common intra-axial tumors in dogs.[1] They are poorly to well marginated, with or without contrast enhancement on T1-weighted images. A ring-enhancing pattern around nonenhancing abnormal tissue is often associated with gliomas.[6,8-10] The accuracy of MRI in correctly identifying gliomas in dogs is 73%.[6] In addition to tumor class, identification of the tumor bed, an affected peritumoral region marking the tumor margins, is essential for surgical planning and prognosis.[4,11,12]

In the last 2 decades, blood-brain barrier dysfunction (BBBD) has been implicated in the pathophysiology of a multitude of neurological diseases, including primary and secondary brain neoplasia, in humans and experimental animals.[13-21] The 2 basic mechanisms of BBB breakdown are transcytosis and paracellular which differ in permeability characteristics as well as time and onset after the insult.[22,23] Moreover, in cases of brain neoplasia, tumor progression is highly associated with abnormal angiogenesis. In gliomas in humans, disease progression of low-grade to high-grade glioma (WHO grade II-IV) is characterized by increased vascularization associated with BBB disturbances. Blood-brain barrier alterations are most prominent in glioblastoma multiforme (WHO IV, GBM), the most malignant brain tumor that is associated with high morbidity and poor median survival.[24] These discoveries have driven technological advances in detection and quantification of BBBD in vivo. Recently developed MRI analysis algorithms allow clinical evaluation of BBBD in both experimental animals and clinical cases.[25-30] T1-weighted dynamic contrast-enhanced (DCE) perfusion MRI (DCE-MRI), which allows quantitative assessment of tissue perfusion over time and BBBD, has already been used in clinical practice to image primary and secondary brain neoplasms and to differentiate meningiomas from dural-based metastases in humans.[31-34] Moreover, peritumoral edema surrounding atypical meningiomas have distinct perfusion characteristics compared with benign meningiomas.[34] In dogs, DCE-MRI enables the identification and quantification of brain areas with BBBD in naturally occurring brain diseases.[25] A less demanding semiquantitative method that was suggested for detecting BBBD is subtraction enhancement analysis (SEA),[35] which compares enhancement in each brain voxel in MR images obtained before and after intravenous contrast administration.

Here, we addressed the hypothesis that application of these 2 BBBD quantification methods can provide clinically useful information on the behavior and class of brain tumors in dogs. For that, we conducted a prospective study to quantify BBBD using DCE-MRI data of extra-axial and intra-axial brain tumors, and a retrospective SEA on MR images of histologically confirmed meningiomas and gliomas.

2 | MATERIALS AND METHODS

2.1 | Animals and study design

This study had 2 arms (Figure 1). In the first arm, we analyzed DCE-MRI data from dogs that participated in a prospective study to assess BBB integrity in various neurological diseases. Dogs with either intra-axial or extra-axial space-occupying lesion, which was diagnosed as a brain tumor by both a radiologist (DP) and a board-certified neurologist (MS), were included. The control group contained 6 healthy shelter dogs admitted for neutering surgery. Inclusion criteria for the control group, were normal physical and neurological examination, normal CBC and chemistry profile, normal cerebrospinal fluid (CSF) cytology, total protein, and no abnormalities on MRI.

The second arm was a retrospective analytical cross-sectional study conducted by archived MRI and medical record data from the Koret School of Veterinary Medicine Teaching Hospital (KSVM-VTH; group i), and from both the University of Veterinary Medicine Hannover (UVM-H) and the Royal Veterinary College (RVC), London (group ii). In group i, MRI records of all dogs admitted to the hospital between 2014 and 2019 with neurological dysfunction were reviewed. Only dogs diagnosed with a brain tumor were included. Medical history, complete physical and neurological examination, CBC, serum biochemical profile, and CSF analysis results were recorded. The control group included 6 dogs that underwent head MRI for evaluation of extracranial diseases. In group ii, MRI of dogs admitted to RVC and the UVM-H between 2001 and 2009 that were diagnosed with brain tumors after MRI evaluation were reviewed. Only dogs in which the tumor class was later

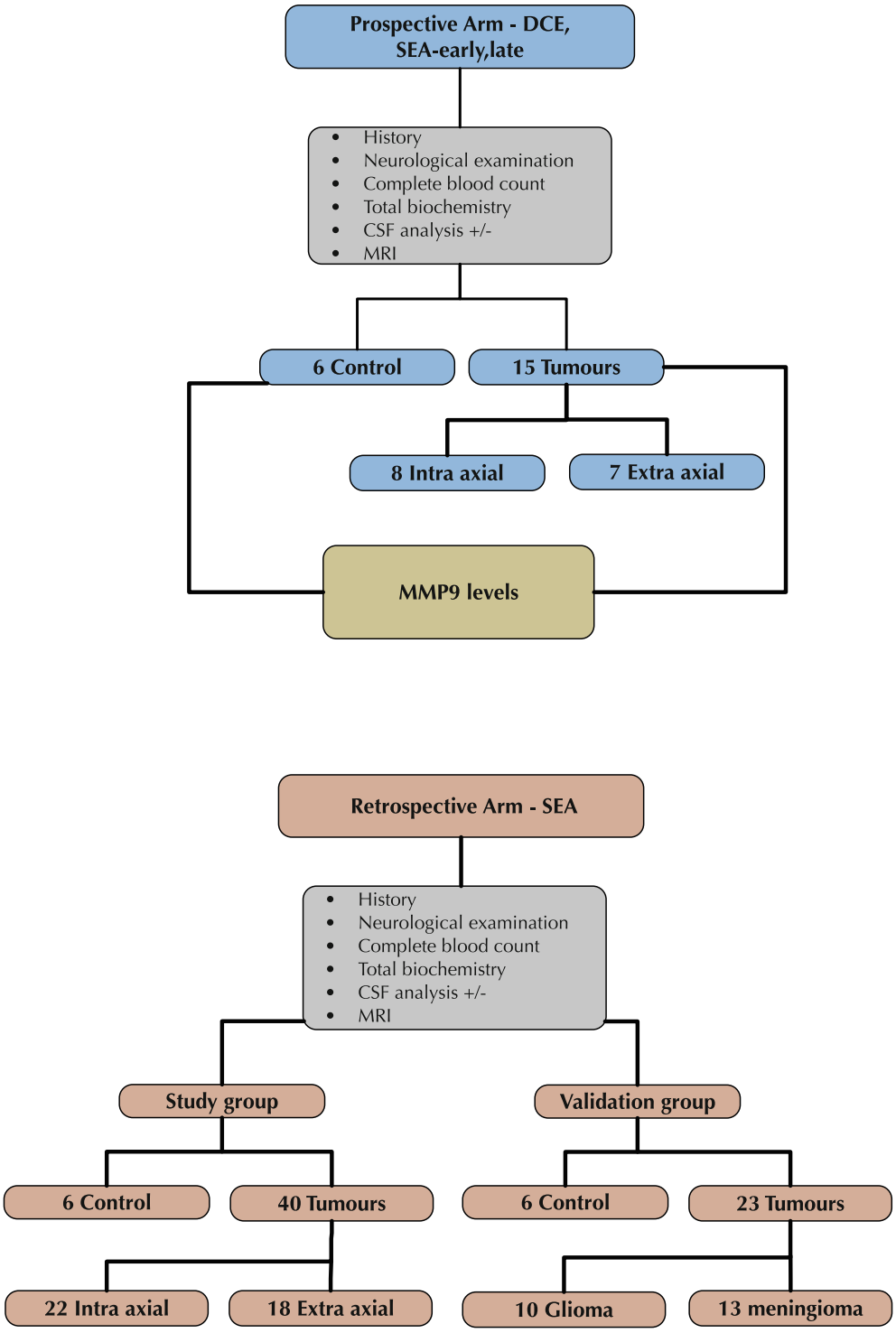

FIGURE 1 Flow chart of the study design showing the 2 arms of the study, namely dynamic contrast enhanced (DCE) and subtraction enhancement analysis (SEA).

confirmed by histopathology to be either a glioma or meningioma were included.

Brain tumors were diagnosed independently by a radiologist (CL) and a neurologist (VH) based on clinical signs of focal space-occupying brain lesion, which appeared as hyperintense lesions on T2-weighted sequences with or without postcontrast T1-weighted sequences.

All procedures were approved by the institutional ethics committee (see Section 2.7).

2.2 | MRI protocols

2.2.1 | DCE prospective analytical cross-sectional study

DCE-MRI protocol

Dynamic contrast-enhanced MRI (DCE-MRI) studies were performed by a 0.35-Tesla magnet (Magentom C, Siemens Healthineers, Berlin,

Germany). Dogs were under general anesthesia maintained with 1% to 2% isoflurane and constant oxygen flow (100%, 2 L/h) after intubation. Seven transverse T1-weighted gradient recalled echo sequences were obtained, 1 before and 6 immediately after contrast administration (TE: 6.75-7.3 ms, TR: 192-445 ms, flip angle: 90°, slice thickness: 3.5-4 mm, interslice gap: 3.85-4.4 mm, FOV: 13.5 × 13.5 cm to 18 × 18 cm, reconstruction matrix: 192 × 192).

SEA protocol

The obtained DCE images were evaluated a second time by the SEA method. For that, 2 postcontrast time points, namely early (SEA_{early}, 5 minutes after contrast administration) and late (SEA_{late}, 30 minutes after contrast administration), were used to calculate the increase in tissue enhancement relative to baseline (precontrast) images. BBB scores were calculated separately for each method and permeability maps were generated.

2.2.2 | MRI protocol for retrospective analytical cross-sectional SEA study

Group i

For SEA, T1-weighted spin echo sequences in the transverse plane acquired before and after the injection of contrast agent were used (TE: 21 ms, TR: 642-916 ms, flip angle: 90°, slice thickness: 3.5-4 mm, interslice gap: 3.85-4.4 mm, FOV: 13.5 × 13.5 cm–18 × 18 cm, reconstruction matrix: 256 × 256–384 × 384).

Group ii

MRI studies were performed by 1.5-Tesla magnet (Gyroscan NT intera, Philips, Eindhoven, Netherlands). Precontrast and postcontrast T1-weighted spin echo sequences in the transverse plane were used (TE: 11-15 ms, TR: 457-719 ms, flip angle: 90°, slice thickness: 3.5-5.0 mm, interslice gap: 2.7-4.5 mm, FOV: 13.5 × 13.5 cm-18 × 18 cm, reconstruction matrix: 160 × 160-512 × 512).

2.3 | Image analysis and quantification of BBBD score

The investigators analyzing the images were blinded to the diagnosis. For BBB quantification, image preprocessing included extracting the whole brain volume by a semi-automatic algorithm and a user who sampled white and gray matter intensity values in the T1-weighted spin echo image. Brain mask was created and extracted automatically by the algorithm. Images were then registered by in-house MATLAB functions to align each postcontrast image to the corresponding precontrast image.

2.3.1 | DCE-MRI analysis

Images of postcontrast T1-weighted gradient echo scans (T1 GE + C_1-6) were analyzed as previously reported.[25] A signal s(t) was fitted to a linear curve such that $s(t) = A \times t + B$, where the slope (A) is the rate of wash-in or wash-out of the contrast agent from the brain parenchyma and (B) is the intercept value, that is, the pick contrast value in $t = 0$ after contrast administration.

Blood-brain barrier permeability map was generated for the whole brain and represented the slope values of each voxel. In addition, the DCE images were used for early and late SEA, as described in the next paragraph.

2.3.2 | SEA image analysis

For SEA, the difference in signal intensity between precontrast and postcontrast scans, presented as percentage from the precontrast value, was calculated for each voxel. This variable was termed the percentage of intensity difference (PID). The mean PID value calculated in each dog for a 2 cm^2 area of the temporal muscle, representing a tissue with no blood-tissue barrier, served as a reference value. Positive voxels, representing permeability, were determined by 2 ranges. Low range (LR) was defined as the range between mean PID of the temporal muscle and the mean plus 1 SD, whereas high range (HR) was defined as equal to or greater than the mean PID of the temporal muscle plus 1 SD.

Blood-brain barrier score was calculated for both DCE and SEA in 3 steps. First, all positive brain voxels were detected as described above. Second, a region-growing procedure was applied to each positive voxel involving repeatedly connecting neighboring voxels. Small noisy clusters (ie, less than 4 neighboring voxels) were removed by morphological filtering procedure. Lastly, BBB score was assigned to each dog by calculating the percentage of positive voxels in their brain images.

Blood-brain barrier score was similarly calculated for all control dogs. The means BBB score calculated for the 6 control dogs plus 2 SDs was set as a threshold for normal BBB (NBBB). Dogs with BBB score above this threshold were considered as suffering from BBBD.

Analysis was performed by in-house MATLAB scripts (MATLAB 2018b, The MathWorks, Inc., Natick, Massachusetts).

2.3.3 | Additional image analyses

Aftr the imaging diagnosis, dogs from group i were allocated to 1 of 2 groups: intra-axial or extra-axial tumors. Tumor volume was estimated by measuring the maximal length of the lesion in axial and coronal postcontrast MRI images. If the 2 measurements were identical, tumor shape was considered a sphere, whereas if 1 diameter was larger the tumor was considered as cylindrical. The volume of each tumor was calculated accordingly.

2.4 | Evaluation of MMP9 activity levels by zymography

Zymography was performed on 21 serum samples, including 15 from dogs with brain tumor and 6 from control dogs. The samples were

centrifuged at 14 000 rcf for 2 minutes at 4°C, incubated for 20 minutes at room temperature, and preserved at −80°C. Protein concentration was normalized according to total protein data. The samples were diluted with loading buffer [0.5 M Tris (pH 7.6), 5% sodium dodecyl sulfate (SDS), 20% glycerol, 0.03% bromophenol blue], and electrophoretically separated on 10% SDS-PAGE gels copolymerized with 1% gelatin. Gels were washed twice with renaturing buffer (0.5 M Tris (pH 7.6), glycine, sterile diH_2O) at 37°C to remove SDS and then washed and incubated with a developing buffer (0.5 M Tris (pH 7.6), 50 mM $CaCl_2$, sterile diH_2O) at 37°C for 16 hours. After staining with Coomassie blue solution (0.1% Coomassie Brilliant Blue R-250, 5% methanol, 10% acetic acid, sterile diH_2O), the gels were destained with solution including 5% methanol, glycerol, and 10% acetic acid in water. When the gelatinolytic bands (MMP9) were visualized, images were taken with an image analyzer (ImageQuant LAS4000mini, Sweden). Blot intensity (92 kDa for MMP9) was quantitatively determined by ImageJ software version 1.5a (National Institute of Health, Bethesda, Maryland).

2.5 | Histopathological confirmation of tumor class

Tumor class was determined histopathologically by a certified pathologist (WB) at the University of Veterinary Medicine Hanover, Germany, and was available in the medical records of included cases.

2.6 | Statistical analysis

Magnetic resonance imaging data were analyzed by an author who was blinded to the group affiliation of the dogs. The Shapiro-Wilk test was used to assess distribution of continuous parameters. Two-sample *F*-test for equal variances was used for quantitative comparisons. To compare quantitative variables between 2 independent groups, the 2-sample *t* test and the nonparametric Mann-Whitney test were used. Pearson's or Spearman's correlation tests were used, as appropriate. Receiver operating characteristic (ROC) analysis was performed to assess the predictive value of the BBB scores for tumor class; result are presented as area under the curve (AUC) and 95% confidence interval (CI). All tests were 1-tailed, and a *P*-value of .05 or less was considered statistically significant. All statistical tests were done by MATLAB scripts (MATLAB 2018b, The MathWorks, Inc., Natick, Massachusetts). Data are presented as mean ± SD.

2.7 | Ethical considerations

All tests performed, including MRI scans, were part of the clinical workup. Additional analyses were done by the raw MRI data obtained from the radiology archive of the institute. The addition of the dynamic sequences for this study and its protocol, as well as the use of healthy shelter dogs as controls, were approved by the Hebrew University Veterinary Teaching Hospital Ethics Committee (approval number KSVM-VTH/26_2016). Written informed consent was obtained from all dog owners to allow prolonging the anesthesia time for additional MRI sequences needed for the study.

3 | RESULTS

3.1 | Characteristics of study cohort and tumor class

Fifteen dogs were included in the prospective DCE-MRI arm of the study, of which 7 had extra-axial tumors and 8 had intra-axial tumors. Male to female ratio was 5/2 in dogs with extra-axial tumors and 7/1 in dogs with intra-axial tumors. The median age of dogs with extra-axial tumors was 9 years (range, 9-15 years) and of dogs with intra-axial tumors it was 8 years (range, 2-12 years). Median body weight was 30 (range, 9-48) kg for dogs with extra-axial tumors and 27.5 (range, 9-53) kg for dogs with intra-axial tumors. Estimated volume of the tumors ranged between 0.07 and 22.5 cm^3 (median, 1.76 cm^3), with no difference between extra- and intra-axial tumors.

The control group included 6 healthy dogs. Males to female ratio of 2/1, median age was 4.5 years (range, 4.5-5) and median body weight was 20.7 kg (range, 5-30 kg).

In group i of the retrospective SEA arm, 40 dogs met the inclusion criteria, of which 18 had extra-axial tumors, and 22 had intra-axial tumors. Male to female ratio was 8/10 for dogs with extra-axial tumors and 10/12 for dogs with intra-axial tumors. The median age of dogs with extra-axial tumors was 9.2 years (range, 4.7-18 years) and of dogs with intra-axial tumors, it was 9 years (range, 4-17 years). Median body weight of dogs with extra-axial tumors was 28 kg (range, 5-38 kg) and of dogs with intra-axial tumors, it was 21.0 kg (range, 5-48 kg). Median estimated tumor volume ranged between 0.09 and 8.5 cm^3 (median, 2.14 cm^3), with no difference between extra- and intra-axial tumors.

In the control group (n = 6), male to female ratio was 5/1, median age was 7 years (range, 5-10 years), and median body weight was 35.5 kg (range, 2-42 kg).

In group ii of the retrospective study, 23 dogs were included in the histopathologically confirmed tumor class group, of which 13 were diagnosed with meningioma and 10 with glioma. Male to female ratio in dogs with meningioma was 6/7 and in dogs with glioma, it was 4/6. Dogs with meningioma were significantly older, with a median age of 10 years (range, 8-12 years) as compared to 7.5 years (range, 6-10 years) for dogs with glioma ($P < .01$, Mann-Whitney *U* Test). Median body weight of dogs with meningioma was 25 kg (range, 6-40 kg) and of dogs with glioma it was 24 kg (range, 6-40 kg).

3.2 | Prospective study arm: Calculation of BBB score by DCE, SEA_{early}, and SEA_{late}

A summary of BBB scores calculated by each of the described methods is given in Table 1. DCE-MRI analysis of the 6 control dogs

TABLE 1 BBB scores calculated by DCE and SEA methods

	DCE	SEA_{early} HR	SEA_{late} HR	SEA_{early} LR	SEA_{late} LR
Extra-axial	18.9 (7.3-44.6)	10.5 (2.7-19.3)	10.4 (6.9-24.1)	1.4 (0.5-1.9)	2.9 (1.5-5.3)
Intra-axial	16.1 (8.7-32.1)	2.1 (0.2-12.6)	3.0 (0.5-13.1)	1.3 (0.1-2.3)	2.4 (0.1-7.1)
Control	16.1 (6.1-25.0)	0.8 (0.2-2.5)	0.8 (0.1-2.5)	0.9 (0.5-1.9)	1.2 (0.3-3.6)
	SEA HR	**SEA LR**	**SEA HR/LR**		
Extra-axial	2.8 (0.2-7.2)	2.0 (0.7-5.3)	0.7 (0.2-4.5)		
Intra-axial	1.4 (0.1-10.2)	2.5 (0.4-6.8)	1.4 (0.2-26)		
Control	0.2 (0-0.3)	0.5 (0.3-1.15)	–		
	SEA HR	**SEA LR**	**SEA HR/LR**		
Meningioma	2.4 (0.6-6.0)	0.09 (0.01-0.24)	0.02 (0-0.08)		
Glioma	2.85 (0.2-14.0)	0.5 (0.02-1.04)	0.13 (0.05-1)		

Note: BBB score calculated as percentage of positive (dysfunctional BBB) voxels, from the whole brain, in parentheses are the range of values.
Abbreviations: DCE, dynamic contrast enhanced; HR, high range; LR, low range; SEA, subtraction enhancement analysis.

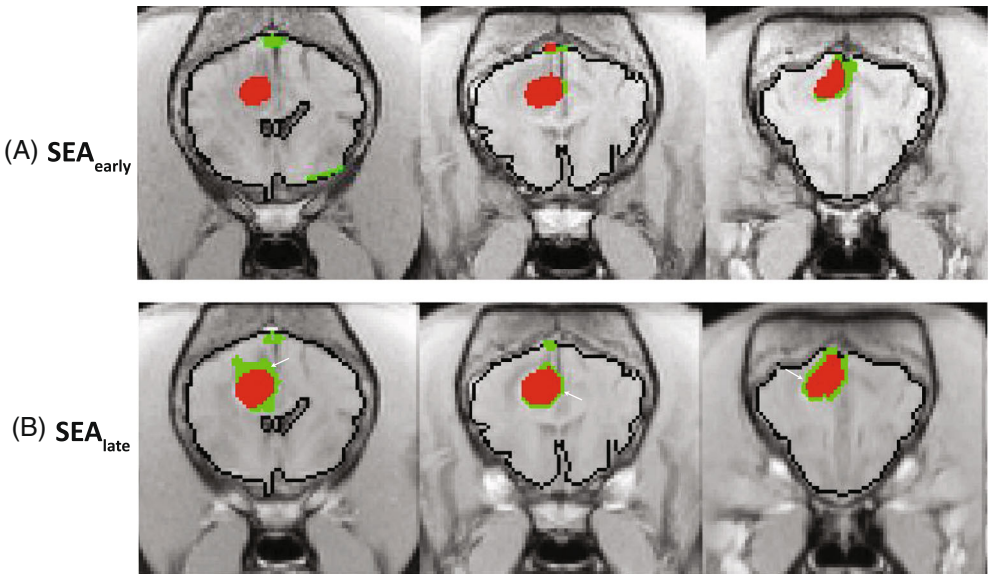

FIGURE 2 Color-coded permeability maps of a canine glioma calculated using SEA at 2 time points following contrast administration and using either high (HR, red) or low (LR, green) thresholds for BBBD. Note the expansion of permeable voxels in the late SEA maps (B, white arrows) as compared to the early SEA maps (A).

yielded a score threshold of 22.19% for NBBB. Using this threshold, only 3 dogs with tumors, 2 with extra-axial and 1 with intra-axial, had higher percentages of positive voxels and were therefore considered as having BBBD.

For SEA on DCE images, high (HR) and low range (LR) for permeable voxels were calculated as previously described, and thresholds of NBBB were based on the HR and LR BBB scores of the control group. These thresholds were set at 2.6% and 2.0% positive voxels, respectively, for the HR SEA_{early} and at 2.6% and 4.2%, respectively, for SEA_{late} (n = 6). For dogs with brain tumor, SEA_{late} BBB score was significantly higher than SEA_{early} score when both HR and LR were used (P = .002 and .002, respectively, paired t test). No such difference was detected in the control dogs (P = .35 and .23, respectively, paired t test; Figure 2).

Ten dogs with tumors (10/15) were identified with BBBD when the HR for SEA_{early} was used, including 7/7 dogs with extra-axial tumors and 3/8 dogs with intra-axial tumors. When using HR for SEA_{late}, BBBD was detected in 11/15 dogs, including again all 7 dogs with extra-axial tumors and 3/8 dogs with intra-axial tumors. When using the LR for SEA_{early}, none of the dogs with extra-axial tumors and only 1/8 dogs with intra-axial tumor were identified as having BBBD. When using the LR for SEA_{late}, 3/7 dogs with extra-axial tumors and 1/8 dogs with intra-axial tumors were identified with BBBD.

The BBB scores calculated for dogs with extra-axial tumors were significantly higher than the scores of dogs with intra-axial tumors when using both SEA_{early} and SEA_{late} in combination with the HR (P = .024 and .024, respectively, Mann-Whitney U Test).

3.2.1 | Permeability maps evaluation

Dynamic contrast-enhanced image-based permeability maps revealed a consistent prominent feature in 6/7 dogs with extra-

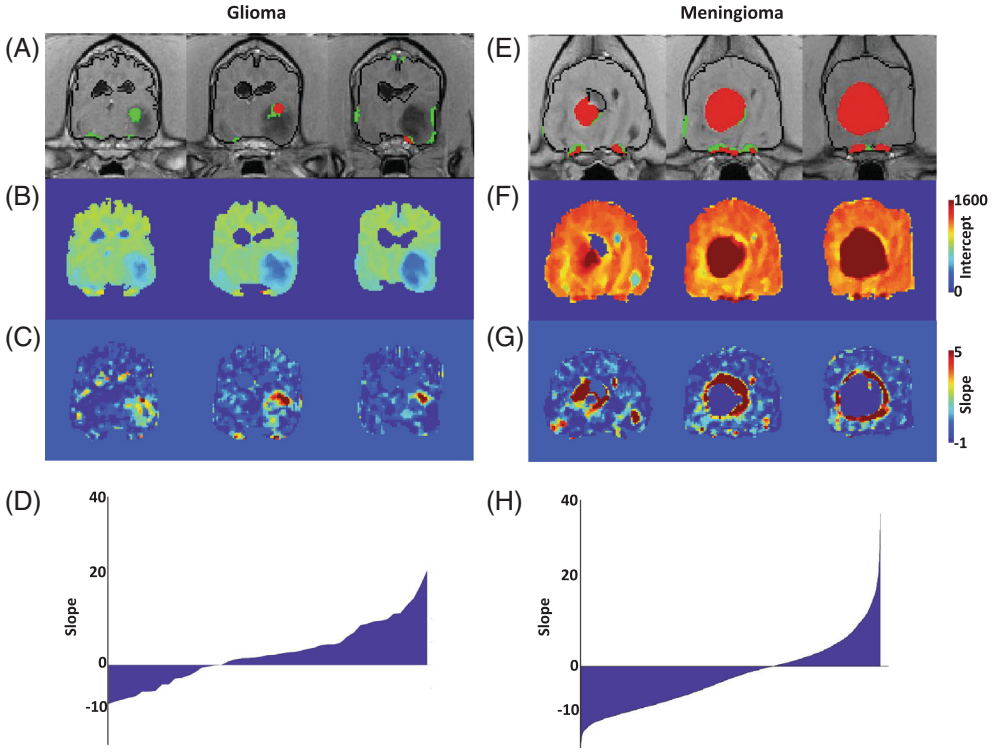

FIGURE 3 SEA and DCE permeability maps of meningioma and glioma. (A) SEAearly permeability map of a dog diagnosed with glioma showing HR-positive voxels (red) and LR positive voxels (green). (B) DCE intercept map showing relative low values in the tumor region. (C) DCE permeability map showing slope values of the tumor region. Note the high slope values in the region identified by SEAearly. (D) Distribution of slope values of HR + LR positive voxels, showing a ratio higher than one between positive and negative slopes. (E) SEAearly permeability map of a dog diagnosed with meningioma showing HR-positive voxels (red) and LR positive voxels (green). (F) DCE intercept map showing relative high values in the tumor region. (G) DCE permeability map showing slope values of the tumor region. Note the negative slope values in most of the region identified by SEAearly. (H) Distribution of slope values of HR + LR positive voxels showing a positive/negative ratio lower than one.

axial tumors. Regions of positive voxels identified by SEA-HR (Figure 3E, red) overlapped with regions of high values in the intercept maps (Figure 3F) and with negative slopes in the DCE maps (Figure 4G, blue). An opposite trend was observed for intra-axial tumors, where more positive slope voxels were found in regions containing positive voxels in the SEA-based maps, indicating more parenchymal leakage rather than an excess of permeable blood vessels (Figure 3).

3.3 | Retrospective study arm: SEA analysis

3.3.1 | Group i: Extra-axial vs intra-axial tumors

Blood-brain barrier scores for dogs in group i of the retrospective SEA arm of the study (n = 40, 18 with extra-axial and 22 with intra-axial tumors) are summarized in Table 1. Blood-brain barrier dysfunction thresholds based on High and low ranges, as calculated in control dogs (n = 6), were found to be 0.31% and 1.29%, respectively. When the HR was used, 16/18 (88%) dogs with extra-axial and 20/22 (90%) of dogs with intra-axial tumors were identified with BBBD. When the LR was used, BBBD was detected only in 12/18 (66%) dogs with extra-axial and 16/22 (73%) dogs with intra-axial tumors. The differences in the occurrence of BBBD between dogs with extra-axial and intra-axial tumors were not significant.

The distribution of HR-positive voxels was mainly within the core of the tumors, whereas LR-positive voxels were found in the periphery of the tumors or diffused throughout the brain parenchyma (Figure 4). Interestingly, a trend toward higher LR/HR ratio (ie, the ratio between BBB scores obtained using the 2 ranges) was found for intra-axial tumors, as compared to extra-axial tumors ($P = 0.1$).

When using the HR, tumor size was found to be correlated with BBB score in dogs with extra-axial tumors, but not in dogs with intra-axial tumors ($r = .81$ vs $r = .33$, Pearson correlation respectively). No correlation between tumor size and BBB score was identified when using the LR.

3.3.2 | Group ii: Meningiomas vs gliomas

Blood-brain barrier scores of dogs in group ii of the retrospective study arm, where tumor class was histologically identified, are presented in Table 1. LR-BBB score and LR/HR ratio were significantly higher in gliomas than in meningiomas, with a median score of 0.51% (range, 0.02%-1.04%) for gliomas and 0.09% for meningiomas (range, 0.006%-0.24%) in the LR ($P < .01$, Mann-Whitney test). The median

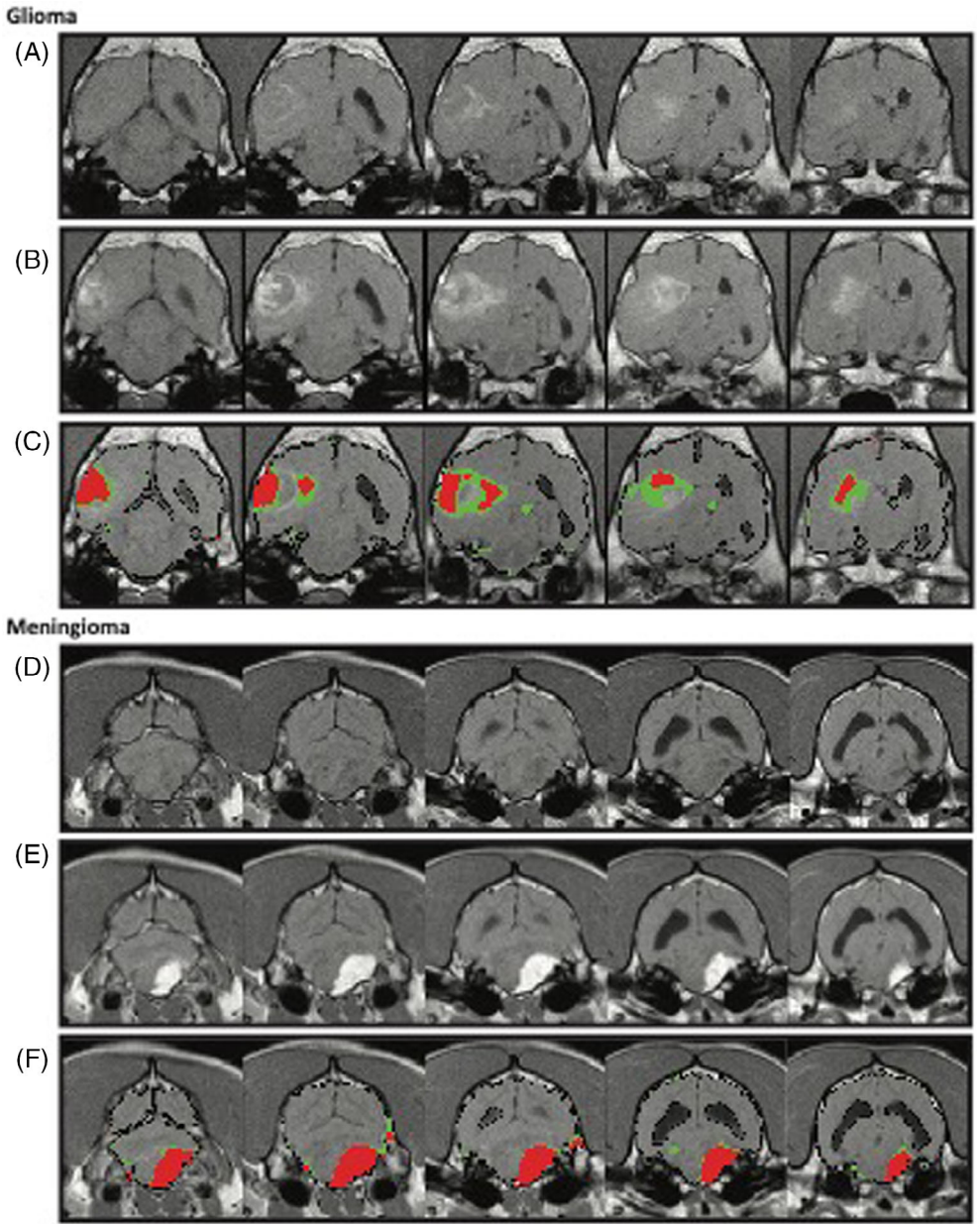

FIGURE 4 Detection of blood-brain barrier dysfunction in dogs with tumors. (A-C) Representation of an intra-axial tumor in a dog. A, Precontrast images; B, postcontrast images; C, positive voxels within the HR (red) or LR (green) range are superimposed on postcontrast T1-weighted images. Note the focal pattern in the center of the lesion in red (HR) and the surrounding parenchyma highlighted in green (LR). (D-F) Representation of an extra-axial tumor in a dog. D, Precontrast images; E, postcontrast images; F, positive voxels of the HR (red) or LR (green) ranges are superimposed on postcontrast T1 weighted images. Note the reduction in perilesional permeable voxels in green (LR) as compared to the intra-axial tumor.

LR/HR ratio was 0.13 (range, 0.05-1.00) for gliomas and 0.02 (range, 0.002-0.075) for meningiomas ($P < .01$, Mann-Whitney test). A sensitivity of 80% and specificity of 100% were calculated for the ability of the SEA LR/HR ratio to distinguish between meningiomas and gliomas (AUC, 0.95 [CI, 0.87-1], cutoff point, 0.10, $P < .01$; Figure 5). HT BBB score alone did not differ significantly between the 2 tumor classes, with a median of 2.43% for meningiomas (range, 0.57%-6.00%) and 2.85% for gliomas (range, 0.16%-14.04%).

3.4 | MMP9 serum levels and their association with BBBD detection

In the serum of dogs with brain tumors, the median MMP9 activity level was 503 a.u. (range, 91-2956 a.u), as compared to 257 a.u. (range, 45-527 a.u) in the control group; however, this difference was not significant ($P = .14$, Mann-Whitney test). Furthermore, no significant differences were found in serum levels of MMP9 when comparing between dogs with extra-axial vs intra-axial tumors using any of the BBB score quantification methods.

4 | DISCUSSION

In this study, 2 advanced imaging analysis methods were used for semiquantification of BBB dysfunction in dogs with brain tumors. Both methods identified BBB leakage in brain areas affected by both gliomas and meningiomas, highlighting a difference in the nature of the BBB dysfunction between the vascular core of the tumor and the surrounding peritumoral tissue. Importantly, the observed differences

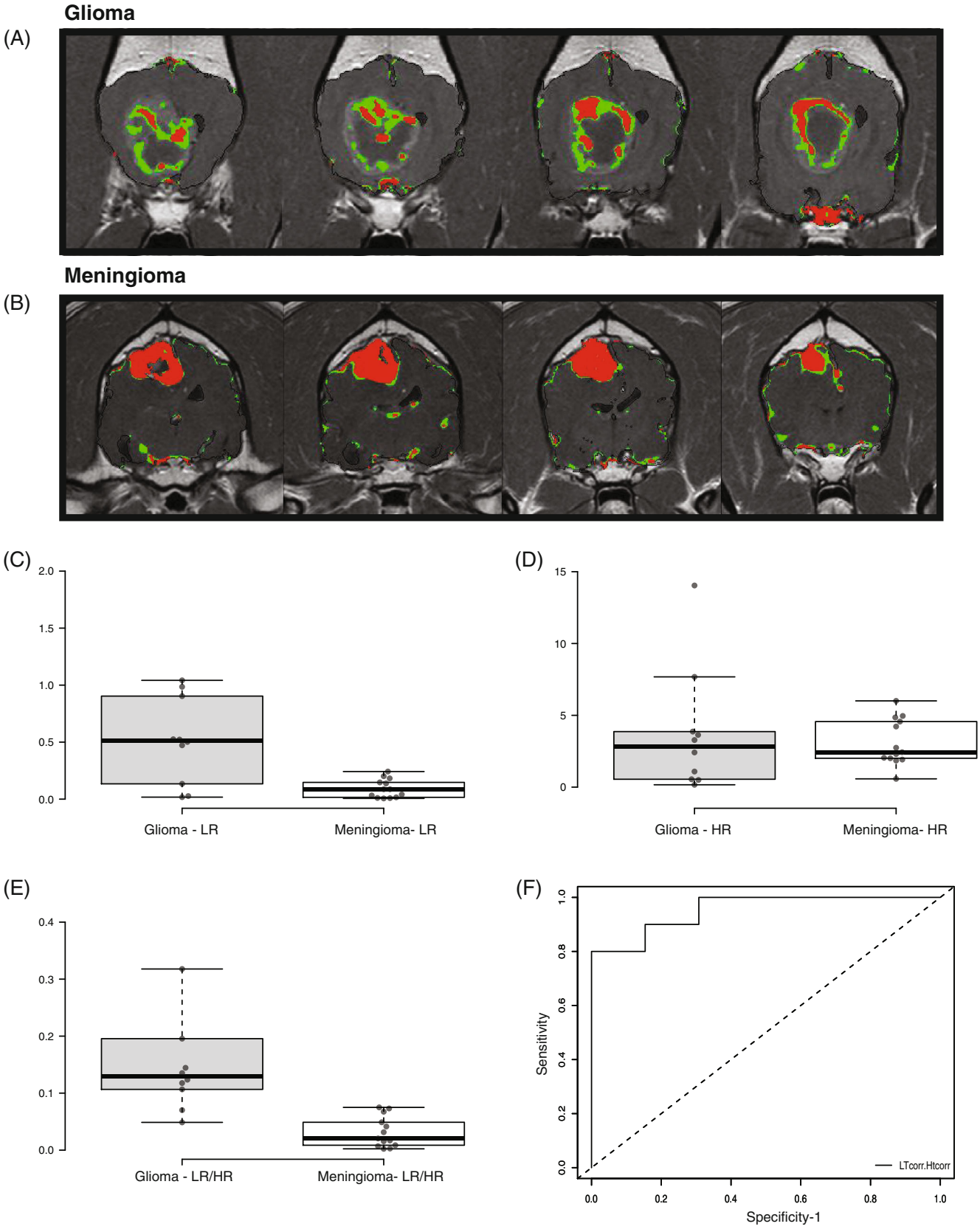

FIGURE 5 Validation of tumor type differentiation using SEA. (A, B) SEA permeability maps of a glioma (A) and meningioma (B) showing HR-positive voxels (red) and LR-positive voxels (green). Note the higher LR/HR ratio in the glioma compared to meningioma. (C-E) Box plots of BBB score of gliomas (G) compared to meningioma (M) using SEA-LR (A), SEA-HR (B), and LR/HR ratio (C). Center lines show the medians; box limits indicate the 25th and 75th percentiles; whiskers extend 1.5 times the interquartile range from the 25th and 75th percentiles. n = 10 (G), 13 (M) sample points. (F) Graph showing receiver operating characteristic (ROC) curve analysis and the sensitivity and specificity of the SEA LR/HR score ratio in detection of tumors type (glioma vs meningioma).

in the extent and distribution of BBB dysfunction between gliomas and meningiomas could be used to help differentiate between the 2 most common classes of brain tumors.

The DCE-MRI modality, which has been described for more than a decade in humans, experimental animals, and, more recently, in dogs is not yet implemented in the routine clinical setup.[25-30] A major limitation of DCE-MRI is the complex imaging requirements, which include initiation of the dynamic sequence before the intravenous contrast injection, followed by repeated scanning. These result in lower spatial resolution and prolongation of anesthesia time, especially in dogs. DCE-MRI detects the accumulation of contrast material in the tissue over time, thereby indicating BBB dysfunction.[25-27] By applying algorithms such as ours to this MRI modality, we and others were able to detect areas of BBBD in subgroups of patients presenting with a variety of neurodegenerative and neuropathological disorders, including brain tumors.[25-27]

By comparison, the pre-post subtraction enhanced analysis (SEA) is a less demanding semi-quantitative method, in which the mean percentage of contrast-enhanced voxels is used to calculate the BBBD score.[26,27] In this method, the postcontrast images are taken within minutes of the IV injection of contrast medium. Thus, the rapid passage of tracer in the arterial phase, which occurs within seconds of the injection and is important mainly for assessment of cerebral blood flow, is overlooked. The fraction of contrast material that lingers in the tissue might provide better evaluation of BBB integrity.[30]

In this study, DCE-MRI-based analysis detected BBBD in only 20% of dogs with tumors, as compared to 66% detection using early SEA and 74% using late SEA. These rates are still lower than could be expected given the known biology and increased blood supply of tumors.[36] Increased sensitivity of BBBD detection was achieved when the images used for the analysis were late postcontrast sequence, allowing more time for the contrast medium to slowly leak through abnormal BBB and accumulate in the tissue. Given the small number of dogs in the control group, it could be that the threshold set to determine BBBD in the DCE-MRI group was high and, consequently, some dogs with dysfunctional barrier were not detected as such. Of these 15 dogs with brain tumors, 40% exhibited serum MMP9 activity that was higher than in control dogs. This proportion is in agreement with published information regarding the use of MMP9 as a biomarker for BBBD in dogs with brain tumors.[37] Therefore, the use of our proposed algorithm might be considered as a preferred method for detecting BBBD in dogs with brain tumors.

In the retrospective arm of the study, we performed SEA on archived MRI data from dogs diagnosed with extra-axial or intra-axial tumors (KSVM-TH) and from dogs with extracranial diseases that served as control. With an aim to differentiate between the various mechanisms of BBB leakage in cases of brain tumor such as the tumor distorted blood vessels, transcytosis, and paracellular leakage, we assessed 2 ranges of permeable voxels definition. The higher range used was less abundant in the control dogs, which resulted in a much higher BBBD detection rate of 90% among the 40 dogs with brain tumors. Using the low range, positive voxels were detected in more control dogs, leading to only 70% detection in dogs with brain tumors. These findings indicate that the high-range SEA is the most sensitive method for the identification of BBBD in dogs with brain tumors. The difference between the results obtained using the 2 ranges might suggest the presence of at least 2 separate mechanisms of BBB leakage. The first might involve passage through the tumor's distorted vasculature, which lacks some elements of the BBB[18,21] allowing, for example, intense and unified tumor enhancement in meningioma. The second and more subtle mechanism might involve transcellular transport, which is also slower.[38] This might explain the significantly higher BBB score calculated when the DCE-based SEA_{late} was used, as compared to SEA_{early}.

Comparison between the DCE to the SEA permeability maps shows that both positive and negative slopes are present on DCE maps in areas detected as permeable voxels by SEA method. Furthermore, in both methods, different intercept values of the slopes were identified for extra- vs intra-axial tumors. The extra-axial tumor presented a ratio greater than 1, meaning more negative slopes combined with high intercept values, which can be explained by the vascularity of these tumors, where faster accumulation and clearance of contrast medium is expected. Conversely, intra-axial tumors presented a ratio of less than 1, meaning more positive slopes combined with low intercept values. This might be explained by the tendency of tumor and BBB to allow gradual leakage of contrast, leading to its accumulation in the brain parenchyma.

Our results show that HR-positive voxels were prevalent at the center of the lesion, whereas LR-positive voxels populated the periphery of the lesion, which was likely the tumor bed. Histological and immunohistochemical studies are needed to further evaluate the morphological and biochemical differences between these 2 regions, as well as their clinical relevance. Nevertheless, this difference in distribution further supports the notion that there is more than 1 mechanism of BBB dysfunction.

Using HR, BBBD was detected in dogs with rather robust leakage, such as in cases of hypervascularization, blood vessel abnormalities, and congestion,[35] even when the overall number of positive voxels was small. The LR, on the other hand, limits the values of positive voxels to the range between the mean PID of the temporal muscle and the mean plus 1 SD and, hence, detects only voxels with mild enhancement. Therefore, a higher percentage of positive voxels are detected in the brains of healthy dogs. Consequently, using the LR is expected to provide less sensitivity but more specificity for subtle leakage through the BBB, rather than to more robust blood vessel abnormalities.

Another difference between the ranges was seen when we analyzed tumor size, which was correlated to the BBB score when using the HR but not when using the LR. Moreover, a correlation coefficient of 0.81 was found between BBB score and tumor size in extra-axial tumors, where most of the blood supply is provided by meningeal vessels, which lack BBB altogether.[29]

Other studies examined the behavior of contrast medium during the first 5 minutes after administration in cases of a canine tumor.[39] The initial area under the gadolinium curve (IAUGC) in these cases reflected the immediate arrival of contrast medium to the tissue

including blood flow, vascular permeability, and the fraction of interstitial space. When DCE is used to study hemodynamics in brain tumors, a promising correlation is seen between the relative cerebral blood volume and both histopathological grade of the tumor and the degree of neovascularization.[39] These measurements are done at the immediate phase after contrast administration, when the contrast material is still within the tumor's abnormally tortuous and dilated blood vessels. In our study, the first postcontrast sequence for SEA was obtained 3.5 to 5 minutes after contrast administration. Hence, it is more likely to represent the accumulation of contrast material in the interstitial space, either because of BBB dysfunction, or because of the newly formed and distorted blood vessels within the tumor.[31]

Regarding tumor class, the ratio between BBB scores calculated by LR and HR was significantly higher in gliomas than in meningiomas. Furthermore, this ratio distinguished between the 2 tumor classes with a sensitivity of 80% and a specificity of 100%. Different patterns of postcontrast enhancement were used to distinguish glioma from meningioma.[40] Our algorithm, as was demonstrated on 23 dogs with histologically confirmed tumor class, might further help differentiating these tumors using a routine MRI protocol. Moreover, identifying the extent and possibly class of BBB permeability within and around the tumor might prove to be essential for assessing prognosis and response to treatment in dogs with gliomas.[22,39]

The main limitations in our study were the lack of histological confirmation of tumor class in the prospective, dynamic arm of the study. Furthermore, using a higher field MRI of 1.5 T for the DCE-MRI analysis could possibly improve the resolution and therefore the identification of permeable voxels.

In conclusion, the advanced image analysis methods presented here can serve both clinicians and researchers as additional tools for characterization and quantification of BBBD in dogs with brain tumors. Whereas DCE-MRI provides additional information about tumor biology, the SEA method detected BBBD in 90% of the dogs. The SEA LT/HT ratio can be used in a clinical setting as an additional tool for differentiating between gliomas and meningiomas. Whereas each method has its advantages and limitations, both were shown to add essential information on the extent and characteristics of BBB leakage in dogs with brain tumors. This information might improve the clinical evaluation of intracranial neoplasia, thereby assisting in diagnosis as well as in surgery planning. When the role of BBBD in the pathogenesis of canine CNS diseases is better understood, this tool could help identify the former as a possible target for therapy.

ACKNOWLEDGMENT

No funding was received for this study.

CONFLICT OF INTEREST DECLARATION

Andrea Tipold serves as Associate Editor for the Journal of Veterinary Internal Medicine. She was not involved in review of this manuscript. No other authors have a conflict of interest.

OFF-LABEL ANTIMICROBIAL DECLARATION

Authors declare no off-label use of antimicrobials.

INSTITUTIONAL ANIMAL CARE AND USE COMMITTEE (IACUC) OR OTHER APPROVAL DECLARATION

Approved by Hebrew University of Jerusalem, The Koret School of Veterinary Medicine, KSVM-VTH/26_2016.

HUMAN ETHICS APPROVAL DECLARATION

Authors declare human ethics approval was not needed for this study.

ORCID

Erez Hanael https://orcid.org/0000-0003-1284-895X
Marco Ruggeri https://orcid.org/0000-0002-0150-8178
Holger Andreas Volk https://orcid.org/0000-0002-7312-638X
Steven De Decker https://orcid.org/0000-0002-2505-2152
Andrea Tipold https://orcid.org/0000-0002-9421-942X

REFERENCES

1. Song RB, Vite CH, Bradley CW, Cross JR. Postmortem evaluation of 435 cases of intracranial neoplasia in dogs and relationship of neoplasm with breed, age, and body weight. *J Vet Intern Med*. 2013;27(5):1143-1152.
2. Snyder JM, Shofer FS, Winkle TJ, Massicotte C. Canine intracranial primary neoplasia: 173 cases (1986-2003). *J Vet Intern Med*. 2006;20(3):669-675.
3. Hayes HM, Priester WA, Pendergrass TW. Occurrence of nervous-tissue tumors in cattle, horses, cats and dogs. *Int J Cancer*. 1975;5(1):39-47.
4. Dickinson PJ. Advances in diagnostic and treatment modalities for intracranial tumors. *J Vet Intern Med*. 2014;28(4):1165-1185.
5. Rossmeisl JH. New treatment modalities for brain tumors in dogs and cats. *Vet Clin North Am Small Anim Pract*. 2014;44(6):1013-1038.
6. Ródenas S, Pumarola M, Gaitero L, Zamora À, Añor S. Magnetic resonance imaging findings in 40 dogs with histologically confirmed intracranial tumours. *Vet J*. 2011;187(1):85-91.
7. Wisner ER, Dickinson PJ, Higgins RJ. Magnetic resonance imaging features of canine intracranial neoplasia: MR imaging of intracranial neoplasia. *Vet Radiol Ultrasound*. 2011;52:S52-S61.
8. Kraft SL, Gavin PR, DeHaan C, Moore M, Wendling LR, Leathers CW. Retrospective review of 50 canine intracranial tumors evaluated by magnetic resonance imaging. *J Vet Intern Med*. 1997;11(4):218-225.
9. Young BD, Levine JM, Porter BF, et al. Magnetic resonance imaging features of intracranial astrocytomas and oligodendrogliomas in dogs: MRI of astrocytomas and oligodendrogliomas. *Vet Radiol Ultrasound*. 2011;52(2):132-141.
10. José-López R, Gutierrez-Quintana R, Fuente C, et al. Clinical features, diagnosis, and survival analysis of dogs with glioma. *J Vet Intern Med*. 2021;35(4):1902-1917.
11. Johnson PJ, Rivard BC, Wood JH, DiRubio ML, Henry JG, Miller AD. Relationship between histological tumor margins and magnetic resonance imaging signal intensities in brain neoplasia of dogs. *Vet Intern Med*. 2022;36:1039-1048.
12. Zach L, Guez D, Last D, et al. Delayed contrast extravasation MRI: a new paradigm in neuro-oncology. *Neuro Oncol*. 2015;17(3):457-465.
13. Abbott NJ, Friedman A. Overview and introduction: the blood-brain barrier in health and disease. *Epilepsia*. 2012;53(Suppl 6):1-6.
14. Varatharaj A, Galea I. The blood-brain barrier in systemic inflammation. *Brain Behav Immun*. 2017;60:1-12.
15. Sweeney MD, Zhao Z, Montagne A, Nelson AR, Zlokovic BV. Blood-brain barrier: from physiology to disease and back. *Physiol Rev*. 2019;99(1):21-78.

16. Erickson MA, Dohi K, Banks WA. Neuroinflammation: a common pathway in CNS diseases as mediated at the blood-brain barrier. *Neuroimmunomodulation*. 2012;19(2):121-130.
17. Lopes Pinheiro MA, Kooij G, Mizee MR, et al. Immune cell trafficking across the barriers of the central nervous system in multiple sclerosis and stroke. *Biochim Biophys Acta*. 2016;1862(3):461-471.
18. Quail DF, Joyce JA. The microenvironmental landscape of brain tumors. *Cancer Cell*. 2017;31(3):326-341.
19. Sarkaria JN, Hu LS, Parney IF, et al. Is the blood–brain barrier really disrupted in all glioblastomas? A critical assessment of existing clinical data. *Neuro Oncol*. 2018;20(2):184-191.
20. Saunders NR, Dreifuss JJ, Dziegielewska KM, et al. The rights and wrongs of blood-brain barrier permeability studies: a walk through 100 years of history. *Front Neurosci*. 2014;8:404.
21. Arvanitis CD, Ferraro GB, Jain RK. The blood–brain barrier and blood–tumour barrier in brain tumours and metastases. *Nat Rev Cancer*. 2020;20(1):26-41.
22. Liebner S, Dijkhuizen RM, Reiss Y, Plate KH, Agalliu D, Constantin G. Functional morphology of the blood-brain barrier in health and disease. *Acta Neuropathol*. 2018;135(3):311-336.
23. Kang EJ, Major S, Jorks D, et al. Blood–brain barrier opening to large molecules does not imply blood–brain barrier opening to small ions. *Neurobiol Dis*. 2013;52:204-218.
24. Louis DN, Perry A, Reifenberger G, et al. The 2016 World Health Organization classification of tumors of the central nervous system: a summary. *Acta Neuropathol*. 2016;131(6):803-820.
25. Hanael E, Veksler R, Friedman A, et al. Blood-brain barrier dysfunction in canine epileptic seizures detected by dynamic contrast-enhanced magnetic resonance imaging. *Epilepsia*. 2019;60(5):1005-1016.
26. Bar-Klein G, Lublinsky S, Kamintsky L, et al. Imaging blood-brain barrier dysfunction as a biomarker for epileptogenesis. *Brain*. 2017;140(6):1692-1705.
27. van Vliet EA, Otte WM, Wadman WJ, et al. Blood-brain barrier leakage after status epilepticus in rapamycin-treated rats I: magnetic resonance imaging. *Epilepsia*. 2016;57(1):59-69.
28. Veksler R, Shelef I, Friedman A. Blood-brain barrier imaging in human neuropathologies. *Arch Med Res*. 2014;45(8):646-652.
29. Weissberg I, Veksler R, Kamintsky L, et al. Imaging blood-brain barrier dysfunction in football players. *JAMA Neurol*. 2014;71(11):1453-1455.
30. Chassidim Y, Veksler R, Lublinsky S, Pell GS, Friedman A, Shelef I. Quantitative imaging assessment of blood-brain barrier permeability in humans. *Fluids Barriers CNS*. 2013;10(1):9.
31. Ivanidze J, Lum M, Pisapia D, et al. MRI features associated with TERT promoter mutation status in glioblastoma. *J Neuroimaging*. 2019;29(3):357-363.
32. Lui YW, Malhotra A, Farinhas JM, et al. Dynamic perfusion MRI characteristics of Dural metastases and meningiomas: a pilot study characterizing the first-pass wash-In phase beyond relative cerebral blood volume. *Am J Roentgenol*. 2011;196(4):886-890.
33. Yang S, Law M, Zagzag D, et al. Dynamic contrast-enhanced perfusion MR imaging measurements of endothelial permeability: differentiation between atypical and typical meningiomas. *Am J Neuroradiol*. 2003;24(8):1554-1559.
34. Zhang H, Rödiger LA, Shen T, Miao J, Oudkerk M. Perfusion MR imaging for differentiation of benign and malignant meningiomas. *Neuroradiology*. 2008;50(6):525-530.
35. Hanael E, Baruch S, Chai O, et al. Detection of blood-brain barrier dysfunction using advanced imaging methods to predict seizures in dogs with meningoencephalitis of unknown origin. *Vet Intern Med*. 2022;36(2):702-712.
36. Jain RK, di Tomaso E, Duda DG, Loeffler JS, Sorensen AG, Batchelor TT. Angiogenesis in brain tumours. *Nat Rev Neurosci*. 2007;8(8):610-622.
37. Mariani CL, Boozer LB, Braxton AM, et al. Evaluation of matrix metalloproteinase-2 and -9 in the cerebrospinal fluid of dogs with intracranial tumors. *Am J Vet Res*. 2013;74(1):122-129.
38. Azarmi M, Maleki H, Nikkam N, Malekinejad H. Transcellular brain drug delivery: a review on recent advancements. *Int J Pharm*. 2020;586:119582.
39. Zhao Q, Lee S, Kent M, Schatzberg S, Platt S. Dynamic contrast-enhanced magnetic resonance imaging of canine BRAIN tumors. *Vet Radiol Ultrasound*. 2010;51:122-129. doi:10.1111/j.1740-8261.2009.01635.x
40. Saloner D, Uzelac A, Hetts S, Martin A, Dillon W. Modern meningioma imaging techniques. *J Neurooncol*. 2010;99(3):333-340.

How to cite this article: Hanael E, Baruch S, Chai O, et al. Quantitative analysis of magnetic resonance images for characterization of blood-brain barrier dysfunction in dogs with brain tumors. *J Vet Intern Med*. 2023;37(2):606-617. doi:10.1111/jvim.16654